

1 **Millennial meridional dynamics of Indo-Pacific Warm Pool**  
2 **during the last termination**

3

4 **Li Lo<sup>1</sup>, Chuan-Chou Shen<sup>1,\*</sup>, Kuo-Yen Wei<sup>1</sup>, George S. Burr<sup>1,2</sup>, Horng-**  
5 **Sheng Mii<sup>3</sup>, Min-Te Chen<sup>4</sup>, Shih-Yu Lee<sup>5</sup>, Meng-Chieh Tsai<sup>1</sup>**

6 <sup>1</sup>High-Precision Mass Spectrometry and Environment Change Laboratory  
7 (HISPEC), Department of Geosciences, National Taiwan University, Taipei  
8 10617, Taiwan ROC

9 <sup>2</sup>NSF-Arizona Accelerator Mass Spectrometry Facility, Department of Physics,  
10 University of Arizona, Tucson, AZ 85721, USA

11 <sup>3</sup>Department of Earth Sciences, National Taiwan Normal University, Taipei  
12 11677, Taiwan ROC

13 <sup>4</sup>Institute of Applied Geosciences, National Taiwan Ocean University, Keelung  
14 20224, Taiwan ROC

15 <sup>5</sup>Research Center for Environmental Changes, Academia Sinica, Taipei  
16 11529, Taiwan ROC

17

18

Revised to *Climate of the Past*

19

2014.11.23

20

21 \*Corresponding Author: Chuan-Chou Shen

22 Email: river@ntu.edu.tw; Tel: 886-2-3366-5878; Fax: 886-2-3365-1917

23

24

25

26

## 27 **Abstract**

28 To develop an in-depth understanding of the natural dynamics of the Indo-  
29 Pacific Warm Pool (IPWP) during the last deglaciation, stacked North- (N-)  
30 and South-IPWP (S-IPWP) thermal and hydrological records over the past 23-  
31 10.5 thousand years (ka) were built using planktonic foraminiferal  
32 geochemistry data from a new core, MD05-2925 (9.3°S, 151.5°E, water depth  
33 1661 m) in the Solomon Sea and eleven previous sites. Ice-volume corrected  
34 seawater  $\delta^{18}\text{O}$  ( $\delta^{18}\text{O}_{\text{SW-IVC}}$ ) stacks show that S-IPWP  $\delta^{18}\text{O}_{\text{SW-IVC}}$  values are  
35 indistinguishable from their northern counterpart through glacial time. The N-  
36 IPWP SST stacked record features an increasing trend of  $0.5\text{ }^{\circ}\text{Cka}^{-1}$  since 18  
37 ka. Its S-IPWP counterpart shows an earlier onset of temperature increase at  
38 19 ka and a strong teleconnection to high-latitude climate in the Southern  
39 Hemisphere. Meridional SST gradients between N- and S-IPWP were 1 to 1.5  
40  $^{\circ}\text{C}$  during the Bølling/Allerød period and  $< 0.5\text{ }^{\circ}\text{C}$  during both Heinrich event 1  
41 and the Younger Dryas due to a warmer S-IPWP. A warm S-IPWP during the  
42 cold events may possibly weaken the southern hemispheric branch of the  
43 Hadley Cell and reduce precipitation in the Asian Monsoon region.

## 44 **1. Introduction**

45 The Indo-Pacific Warm Pool (IPWP) is the largest warm water mass in the  
46 world, with an annual average sea surface temperature (SST) greater than 28  
47 °C (Yan et al., 1992). Vigorous regional atmosphere circulation transports  
48 latent heat and water moisture from the IPWP to the middle and high latitudes  
49 (Yan et al., 1992). For the past five decades, the IPWP has experienced  
50 surface water freshening and a westward shift in precipitation, resulting in  
51 regional drought in East Africa and storm track changes in East Australia  
52 (Cravatte et al., 2009; Williams and Funk, 2011). Since the early 2000s,  
53 intensive paleoclimatological studies have been conducted to understand  
54 long-term thermal and hydrological changes in the IPWP, associated with  
55 glacial/interglacial (G/IG) cycles, and to constrain the relationship between  
56 warm pool thermal and hydrological fluctuations to high latitude ice sheet and  
57 greenhouse gas concentrations during the late Pleistocene (e.g., Lea et al.,  
58 2000; Stott et al., 2002; Visser et al., 2003; Rosenthal et al., 2003; Stott et al.,  
59 2004; de Garidel-Thoron et al., 2005; Steinke et al., 2006; Levi et al., 2007;  
60 Xu et al., 2008; Linsley et al., 2010; Bolliet et al., 2011; Mothadi et al., 2014).

61 Stacked IPWP SST and seawater oxygen isotope ( $\delta^{18}\text{O}_{\text{SW}}$ ) records from  
62 the last glacial to the Holocene clearly show a close link between the IPWP  
63 SST, the Asian-Australian Monsoon (AAM) system, and sea level (Stott et al.,  
64 2004; Oppo et al., 2009; Linsley et al., 2010). However, a complicated ocean-  
65 island configuration and regional topography hinder the fidelity of using these  
66 records to describe past climate changes in detail (Griffiths et al., 2009;  
67 Mohtadi et al., 2011). In particular, little is known about the meridional

68 thermal-hydrological dynamics between the N-IPWP and S-IPWP during the  
69 last termination.

70 Here we present new oceanic proxy-inferred SST and ice volume-corrected  
71 surface seawater oxygen isotope  $\delta^{18}\text{O}$  ( $\delta^{18}\text{O}_{\text{SW-IVC}}$ ) records from the Solomon  
72 Sea, Papua New Guinea (PNG) for the past 23-10.5 thousand years ago (ka,  
73 before 1950 AD, hereafter). New SST and  $\delta^{18}\text{O}_{\text{SW-IVC}}$  stacked records since  
74 the last termination are built for both the N- and S-IPWP to understand  
75 regional thermal-hydrological changes and interhemispheric teleconnections.

76

## 77 **2. Material and Methods**

78 Site MD05-2925 (9.3°S, 151.5°E, water depth 1661 m) is located at the  
79 northern slope of the Woodlark Basin in the Solomon Sea, which is the  
80 passage of surface and subsurface water masses between low- and middle-  
81 latitude South Pacific Ocean gyre and cross equatorial currents (Grenier et al.,  
82 2011; Melet et al., 2011) (Fig. 1). The seasonal precipitation in this region (Fig.  
83 1) is dominated by the AAM system, coupled with the intertropical  
84 convergence zone (ITCZ) (Shiau et al., 2012, and references therein). Tests  
85 of single species planktonic foraminifera, *Globigerinoides sacculifer* (> 500  $\mu\text{m}$ ,  
86 total amount of 2-6 mg), at 13 selected depths were picked for accelerator  
87 mass spectrometry (AMS)  $^{14}\text{C}$  dating. The AMS dates were calibrated using  
88 the CALIB 6.0.1 program (Stuiver et al., 2010, Table 1; Reimer et al., 2009) to  
89 reconstruct an age model for a time interval from 23 to 10.5 ka.

90 Forty to sixty individuals of the planktonic foraminifera *Globigerinoides*  
91 *ruber* (white, s.s., 250-300  $\mu\text{m}$ ) were picked under the microscope. For Mg/Ca  
92 measurements, 20-30 individuals were gently crushed and transported into a

93 1.5 mL Teflon vial. The cleaning procedure was as follows: (1) foraminiferal  
94 fragments were immersed in ethanol, (2) a 0.45 mL aliquot of 3% H<sub>2</sub>O<sub>2</sub>, (3)  
95 NH<sub>4</sub>Cl (0.45 mL, 1.0 N), (4) NH<sub>2</sub>OH (0.45 mL, 0.01 N), and then (5) dilute  
96 nitric acid (1 mL, 0.005 N). A sector field inductive coupled plasma mass  
97 spectrometer (SF-ICP-MS), Thermo Electron Element II, housed at the High-  
98 Precision Spectrometry and Environment Change Laboratory (HISPEC),  
99 Department of Geosciences, National Taiwan University, was used to  
100 determine trace element/Ca ratios following the methodology developed by  
101 Shen et al. (2007). The detailed cleaning procedure and methodology are  
102 available in Lo et al. (2014). Two-year 1-sigma reproducibility of Mg/Ca  
103 analyses is ±0.21% (Lo et al., 2014). We used a composite Mg/Ca-SST  
104 equation by Anand et al. (2003) to calculate SSTs.

105 For oxygen stable isotope analysis, 7-10 individuals were immersed in  
106 methanol, ultrasonicated for 10 seconds, and then rinsed with deionized water  
107 5 times. Samples were immersed afterward in a hyperchloride sodium (NaOCl)  
108 for 24 hours, and then analyzed with an isotopic ratio mass spectrometer  
109 (IRMS), Micromass IsoPrime, housed in the National Taiwan Normal  
110 University. Long-term 1-sigma precision is better than ±0.05‰ (N = 701, Lo et  
111 al., 2013) with respect to Vienna Pee Dee Belemnite (VPDB).

112 To extract seawater δ<sup>18</sup>O (δ<sup>18</sup>O<sub>SW</sub>) values, we used a cultural based  
113 equation, SST = 16.5 - 4.8 × (δ<sup>18</sup>O<sub>C</sub> - δ<sup>18</sup>O<sub>SW</sub>) (Bemis et al., 1998) and a  
114 constant offset of 0.27‰ between carbonate VPDB and Vienna Standard  
115 Ocean Water (VSMOW) scales. Ice volume corrected δ<sup>18</sup>O<sub>SW</sub> (δ<sup>18</sup>O<sub>SW-IVC</sub>) was  
116 calculated using the method proposed by Waelbroeck et al. (2002).

117 The empirical orthogonal function (EOF) analysis of a modern SST dataset  
118 (1950-2004 AD, Reynolds et al., 2002) for a sector from 20°S – 20°N, and  
119 100°E- 180°E was conducted (Fig. 2) to determine the boundary between N-  
120 and S-IPWP. With an equatorial border, the EOF1 factor (83.4%) clearly  
121 resolved different SST variation groups. The EOF2 factor shows minor (9.7%)  
122 but significant inter-annual zonal (ENSO) control on the SST patterns. EOF  
123 results show that the geographic equator is also the thermal equator between  
124 N-IPWP and S-IPWP (Fig. 2).

125 To build a stacked N- and S-IPWP record, we followed the suggestions by  
126 Leduc et al. (2010) and considered three criteria for this dataset: (1) sites with  
127 locations from 12°N to 15°S, which is the main IPWP range (Yan et al., 1992;  
128 Gagan et al., 2004), and (2) usage of specific proxies, Mg/Ca-derived SST  
129 and  $\delta^{18}\text{O}_c$  records of planktonic foraminifera, *G. ruber* (white, s.s.). Records  
130 from 12 sites were selected, including this study (Table 2). We adopted the  
131 published age model for sites ODP806, MD97-2140, MD97-2141, MD98-2162,  
132 MD98-2170, MD98-2176, and MD98-2181. For records with available original  
133 radiocarbon ages from sites, including MD01-2378, MD01-2390, MD98-2165,  
134 and MD06-3067, we recalculated the age models using the CALIB 6.0.1  
135 program. The sea level change effect on  $\delta^{18}\text{O}_{\text{SW}}$  was also corrected. We  
136 divided the total data into 400-yr windows and calculated the mean and  
137 standard error of the mean for each time window.

138

### 139 **3. Results and Discussion**

#### 140 **3.1 Geochemical proxy data at site MD05-2925**

141 Planktonic foraminiferal geochemical proxy data for site MD05-2925 are  
142 shown in Figure 3. *G. ruber*  $\delta^{18}\text{O}_\text{C}$  varies from -1.0 to -2.3‰ and shows no  
143 significant millennial timescale variations. Mg/Ca ratios feature stable glacial  
144 values of ~3.5 mmol/mol and rapid increasing transitions of 0.5-1.0 mmol/mol  
145 at ~18.5, 16.5, 14.5, and 12.8 ka. The glacial-interglacial variation of  
146 calculated seawater  $\delta^{18}\text{O}_\text{SW}$  changes is ~1‰. Two abrupt decreases of 0.6-  
147 0.8‰ are observed at 14.6 and 11.8 ka.

148

### 149 **3.2 Solomon SST and $\delta^{18}\text{O}_\text{SW-IVC}$ records during the last termination**

150 Mg/Ca SST records of the planktonic foraminifera *G. ruber* reveal a stable  
151 glacial thermal condition during the period 23.0-18.5 ka, with a variation <1 °C  
152 and a glacial-interglacial difference of ~3 °C between the last glacial maximum  
153 (LGM) and the end of the Younger Dryas (YD) in the Solomon Sea (Fig. 4A).  
154 This record is characterized by (i) the end of glacial conditions at 18.5 ka, and  
155 (ii) rapid SST increases of 1-2 °C at 18.5-18.0, 17.0-16.0, 15.0-14.5, and 13.0-  
156 12.5 ka.

157 The onset of deglacial SST increases in this region is consistent with the  
158 timing of thermal changes in the Southern Ocean as inferred from Antarctic  
159 ice core  $\delta\text{D}$  records (Stenni et al., 2003) (Fig. 4A). This agreement indicates a  
160 strong climatic teleconnection between low- and high-latitude realms in the  
161 Southern Hemisphere (SH), as well as change of greenhouse gas  
162 concentrations (Mothadi et al., 2014). There are significant SST increases of  
163 1-2 °C during Heinrich event (H1) and the YD. Previous studies from the  
164 Eastern Equatorial and South Pacific reveal a mechanism characterized by  
165 early warming of South Pacific subtropical mode water (Pahnke et al., 2003;

166 Lamy et al., 2004; Pena et al., 2008). This warm signal is transported along a  
167 gyre to the east equatorial Pacific (EEP) and eventually to the west Pacific  
168 through ocean tunneling (Pena et al., 2008; Qu et al., 2013, Fig. 4A). Our new  
169 SST record is similar to those in the EEP (Pena et al., 2008) and eastern  
170 Indian Ocean records (Xu et al., 2008; Mothadi et al., 2014) for both  
171 termination timing (within dating error) and significant warming during the H1  
172 and YD events. There is a slightly warming ( $<1$  °C) interval at 14.5-13.5 ka  
173 during the B/A period (Fig. 4A). The warming could be attributed to a possible  
174 mixing with the warm N-IPWP surface water.

175 The Solomon Sea  $\delta^{18}\text{O}_{\text{SW-IVC}}$  record is given in Figure 4B. It varies from -  
176 0.5 to 0.1‰ during 23.0-10.5 ka. A relatively stable condition with 1-sigma  
177 variability of 0.1‰ occurred from 23.0 to 16.0 ka. Two significant positive  
178 excursions with 0.2-0.5‰ enrichments in  $\delta^{18}\text{O}$  are observed in the intervals  
179 16.8-15.0, and 13.8-11.8 ka. Two stable periods with low  $\delta^{18}\text{O}_{\text{SW-IVC}}$  of -0.4‰  
180 occurred between 15.0-13.0 ka and after 11.8 ka.

181 The dramatic  $\delta^{18}\text{O}_{\text{SW-IVC}}$  increases during H1 and the YD likely resulted  
182 from a weakening and/or southward shift of the ITCZ (Chiang and Bitz, 2005;  
183 Broccoli et al., 2006), and local evaporation may also play a role. Agreement  
184 of  $\delta^{18}\text{O}$  sequences of Greenland NGRIP ice core and the Solomon Sea  
185  $\delta^{18}\text{O}_{\text{SW-IVC}}$  indicates an imprint from high latitude Northern Hemisphere (NH)  
186 during the last termination period (Shakun and Carlson, 2010) (Fig. 4B).

187

### 188 **3.3 Millennial timescale variations of N- and S-IPWP SST stacks**

189 Both N- and S-IPWP stacked SSTs show the same difference of  $\sim 3$  °C  
190 between the last glacial and interglacial states (Fig. 5A). N-IPWP stacked SST



191 values increased steadily since 18 ka through the termination at a rate of 0.5  
192 °C/kyr. Millennial timescale variability is absent in this record, which is similar  
193 to Linsley et al. (2010) and Stott et al. (2002). Although the resolution of ODP  
194 806 and MD97-2140 are less than our request to solve millennial-timescale  
195 event, there is no significant difference with/without their records in our N-  
196 IPWP stacks (not shown).

197 The onset of the termination at ~19 ka in the S-IPWP stack is consistent  
198 with temperature increases in Antarctica (Stenni et al., 2003), and occur about  
199 1 kyr earlier than in the N-IPWP stack (Fig. 5A). This timing is synchronous  
200 with EEP (Pena et al., 2008) and non-upwelling region eastern Indian Ocean  
201 (Xu et al., 2008; Mothadi et al., 2014) SST records. Thus, our MD05-2925 and  
202 S-IPWP stacked SST may not severely controlled by the equatorial upwelling  
203 intensity. Instead of that, S-IPWP stacked SST represents broad SH  
204 equatorial region thermal conditions under upwelling/non-upwelling, E-W  
205 equatorial and even in the different ocean basin (Indian/Pacific Ocean). The  
206 S-IPWP stacked SST record is characterized by a warming trend during H1  
207 and the YD periods, similar to Antarctic ice core temperature records (Stenni  
208 et al., 2003), and a steady thermal condition at ~27 °C during Bølling/Allerød  
209 (B/A), corresponding to the Antarctic Cold Reversal (ACR) (Fig. 5A).

210 The thermal gradient between N- and S-IPWP is around 1 °C during 23 to  
211 19 ka. Due to the earlier S-IPWP warming, the thermal gradient dropped from  
212 1 to 0.5 °C around 19-18 ka, and persisted to the end of the H1 event. The  
213 largest observed thermal gradient (1.5-2.0 °C) occurred during the B/A period,  
214 and was followed by a 1 °C drop during the YD. The meridional SST gradient  
215 between N- and S-IPWP over the last termination is attributed to the large

216 thermal variability in the S-IPWP (Fig. 5A). Asynchronicity between persistent  
217 N-IPWP and fluctuating S-IPWP SST sequences (Fig. 5A) indicates a  
218 meridionally dynamic IPWP through the last termination period. This N-S SST  
219 gradient variability would also affect interhemispheric air flow and heat  
220 transport (Gibbons et al., 2014; McGee et al., 2014), providing a mechanism  
221 to explain heat transport between the hemispheres on a millennial timescale.

222

### 223 **3.4 N- and S-IPWP $\delta^{18}\text{O}_{\text{SW-IVC}}$ records**

224 Both N- and S-IPWP  $\delta^{18}\text{O}_{\text{SW-IVC}}$  records feature (i) low values of -0.3-0.0‰  
225 during glacial times, and (ii) increasing trends after 19 ka (Fig. 5C). The  
226 gradient between N- and S-IPWP gradually increased from 0‰ to 0.2‰  
227 through the termination (Fig. 5D). A similar pattern of  $\delta^{18}\text{O}_{\text{SW-IVC}}$  between N-  
228 and S-IPWP suggests that hydrological conditions in the two regions were  
229 governed by the same factor(s), probably related to Northern Atlantic cold  
230 perturbations (Shakun and Carlson, 2010). It has also been suggested that a  
231 major  $\delta^{18}\text{O}_{\text{SW-IVC}}$  increase during the H1 and YD periods in the IPWP region  
232 likely resulted from reduced precipitation and oceanic advection in both the N-  
233 IPWP and S-IPWP regions (Gibbons et al., 2014; McGee et al., 2014).

234

### 235 **3.5 Meridional IPWP SST gradient and the southward-shifted ITCZ** 236 **precipitation boundary**

237 A striking feature of the stacked SST records is the warming in the S-IPWP  
238 during the H1 and YD periods (Fig. 5A). Observations over the past six  
239 decades (Fig. 12 of Feng et al., 2013) show that an equatorward shift of the  
240 NH convection branch of the Hadley Cell (HC) could result from an oceanic

241 warming at  $\sim 10^\circ$  S. This equatorward shift could induce a southward ITCZ  
242 shift of about  $10^\circ$  (Feng et al., 2013). Model simulations (Chiang and Bitz,  
243 2005; Broccoli et al., 2006, Lee et al., 2011) suggest that this altered  
244 circulation is a powerful teleconnection between the NH and SH climate  
245 systems through a coupled tropical ocean-atmosphere pathway, and is  
246 supported by marine and terrestrial hydrological proxy data (Wang et al., 2001,  
247 Lea et al., 2003, Wang et al., 2007, Griffiths et al., 2009, Shakun and Carlson,  
248 2010, Mohtadi et al., 2011, Meckler et al., 2012, Ayliffe et al., 2013, Carolin et  
249 al., 2013, Gibbons et al., 2014; McGee et al., 2014, Fig. 6).

250 Distinctly different precipitation conditions across  $8-10^\circ$ S in the IPWP  
251 during the H1 and YD events are illustrated in Figure 6. For example,  
252 enhanced terrestrial sediment flux into the Coral Sea is suggested by a  
253 marine sediment thorium isotopic proxy record at  $11^\circ$  S (Shiau et al. 2011).  
254 Lynch's crater records from northeastern Australia at  $17^\circ$  S (Muller et al., 2008)  
255 show strong Australian summer monsoonal conditions. Stalagmite  $\delta^{18}\text{O}$   
256 records at Flores Island ( $8^\circ$  S) also feature intense precipitation during H1 and  
257 the YD (Griffiths et al., 2009, Ayliffe et al., 2013). However, marine and  
258 stalagmite  $\delta^{18}\text{O}$  evidence reveal conditions of reduced precipitation and  
259 increased salinity in the northern IPWP north of  $8-10^\circ$  S, including the South  
260 China Sea ( $12^\circ$  N, Stenike et al., 2006), Sulu Sea ( $8^\circ$  N, Rosenthal et al.,  
261 2003), Philippine Sea ( $6^\circ$  N, Stott et al., 2002; Boillet et al., 2011), Java Island  
262 ( $8^\circ$  S, Mohtadi et al., 2011), Solomon Sea ( $9^\circ$  S, this study), and Borneo island  
263 ( $4^\circ$  N, Meckler et al., 2012, Carolin et al., 2013) (Fig. 6). On the basis of  
264 previous terrestrial and marine hydrological records and our new data, as well  
265 as modern (Feng et al., 2013) and simulated (Chiang and Bitz, 2005; Broccoli

266 et al., 2006) data, we speculate a sharp precipitation boundary between the  
267 maritime continents and Australia at about 8-10° S, extending from the  
268 Solomon Sea, Arafura Sea and Timor Sea, to the eastern Indian Ocean  
269 during H1 and the YD periods (Fig. 6). We propose that the west and east  
270 boundaries are between the Java-Flores islands (Griffiths et al., 2009,  
271 Mohtadi et al., 2011), and Solomon-Coral Seas, respectively (Shiau et al.,  
272 2011, this study). Geographical pattern mismatch between thermal and  
273 precipitation could be associated with the local convection branch shifting and  
274 sea level change (Linsley et al., 2010).

275 To sum up our geochemical and composite dataset in the IPWP region  
276 during the last terminations, we propose that the enlarged IPWP meridional  
277 SST gradient could result in an altered HC and reduced (increased)  
278 precipitation for the East Asian (Australia) monsoon territories during the H1  
279 and YD periods (McGee et al., 2014). We also propose that variations in the  
280 meridional IPWP SST gradient during the termination period were mainly  
281 caused by the S-IPWP, which is closely linked to high-latitude climate  
282 systems.

283

#### 284 **4. Conclusions**

285 Our new MD05-2925 marine geochemical records and previous reports  
286 suggest that the meridional IPWP thermal conditions are strongly linked to  
287 interhemispheric high-latitude climate during the last deglaciation. Ice volume-  
288 corrected  $\delta^{18}\text{O}_{\text{SW}}$  stacked records show an increasing salinity gradient  
289 between N- and S-IPWP over the last termination. Here we propose a new  
290 process of the thermal evolution of IPWP region, which meridional differences

291 of its thermal gradient could amplify the signal from high latitude Northern  
292 hemisphere climate events and radiative forcing from greenhouse gases. A  
293 hypothetical precipitation boundary around 8-10° S during H1 and the YD has  
294 also been proposed, which is most likely caused by the meridional IPWP SST  
295 gradient and HC anomalies. More advanced high-resolution regional model  
296 simulations are required to clarify (1) local precipitation variation in response  
297 to the complicated sea level and convection change, (2) the role of IPWP  
298 meridional thermal-hydrological gradient to an altered HC, and (3) its  
299 relationship with regional and global climate systems during global climate  
300 perturbation events.

301

302 **Acknowledgements**

303

304 MD05-2925 site location was selected by Min-Te Chen and Meng-Yang Lee  
305 and collected during the IMAGES PECTEN Cruise, conducted by Luc  
306 Beaufort and Min-Te Chen. Chien-Ju Chou, Wan-Lin Hu, and Yu-Ting Hsiao  
307 helped to pick foraminifera samples. Yang-Hui Hsu helped to operate the  
308 climatological database and plotted figures. Thanks to Delia W. Oppo and  
309 Braddock K. Linsley for their generous offering of the non-overlapping method  
310 MatLab code. This research was funded by Taiwan ROC MOST (99-2611-M-  
311 002-005, 100-2116-M-002-009 and 103-2119-M-002-022 to CCS; 95-2611-M-  
312 002-019 and 96-2611-M-002-019 to KYW), and National Taiwan University  
313 (101R7625 to CCS).

314

315 **References**

- 316 Anand, P. A., Elderfield, H., and Conte, M. H.: Calibration of Mg/Ca  
317 thermometry in planktonic foraminifera from a sediment trap time series.  
318 *Paleoceanography*, 18, 1050, doi:10.1029/2002PA000846, 2003.  
319
- 320 Ayliffe, L. K., Gagan, M. K., Zhao, J.-x., Drysdale, R. N., Hellstrom, J. C.,  
321 Hantoro, W. S., Griffiths, M. L., Scott-Gagan, H., Pierre, E. S., Cowley, J. A.,  
322 and Suwargadi, B. W.: Rapid interhemispheric climate links *via* the  
323 Australasian monsoon during the last deglaciation. *Nature Commun.*, 4,  
324 doi: 10.1038/ncomms3908.
- 325
- 326 Bolliet, T., Holbourn, A., Kuhnt, W., Laj, C., Kissel, c., Beaufort, L., Kienast, M.,  
327 Andersen, N., and Garbe-Schönberg, D.: Mindanao Dome variability over  
328 the last 160 kyr: Episodic glacial cooling of the West Pacific Warm Pool.  
329 *Paleoceanography*, 26, PA1208, doi: 10.1029/2010PA001966, 2011.  
330
- 331 Broccoli, A. J., Dahl, K. A., and Stouffer, R. J.: Response of the ITCZ to  
332 Northern Hemisphere cooling. *Geophys. Res. Lett.*, 33, L01702, doi:  
333 10.1029/2005GL024546, 2006.  
334
- 335 Carolin, S. A., Cobb, K. M., Adkins, J. F., Clark, B., Conroy, J. L., Lejau, S.,  
336 Malang, J., and Tuen, A. A.: Varied response of Western Pacific hydrology  
337 to climate forcings over the last glacial period. *Science*, 340, 1564-1566,  
338 2013.  
339
- 340 Chiang, J. C. H., and Bitz, C. M.: Influence of high latitude ice cover on the  
341 marine Intertropical Convergence Zone. *Clim. Dynam.*, 25, 477–496, 2005.  
342
- 343 Cravatte, S., Delcroix, T., Zhang, D., McPhaden, M., and Leloup, J.: Observed  
344 freshening and warming of the western Pacific Warm Pool. *Clim. Dynam.*,  
345 33, 565–589, 2009.  
346
- 347 de Garidel-Thoron, T., Rosenthal, Y., Bassinot, F., and Beaufort, L., (2005),  
348 Stable sea surface temperatures in the western Pacific warm pool over the  
349 past 1.75 million years. *Nature*, 433, 294–298, 2005.  
350
- 351 Feng, J., Li, J., and Xie, F.: Long-term variation of the Principal mode of  
352 boreal spring Hadley Circulation linked to SST over the Indo-Pacific Warm  
353 Pool. *J. Clim.*, 26, 532-544, 2013.  
354
- 355 Gibbons, F. T., Oppo, D. W., Mohtadi, M., Rosenthal, Y., Cheng, J., Liu, Z.,  
356 and Linsley, B. K.: Deglacial  $\delta^{18}\text{O}$  and hydrological variability in the tropical  
357 and Indian Oceans. *Earth Planet. Sci. Lett.*, 387, 240-251, 2014.  
358
- 359 Grenier, M., Cravatte, S., Blanke, B., Menkes, C., Joch-Larrouy, A., Durand,  
360 F., Melet, A., and Jeandel, C.: From the western boundary currents to the  
361 Pacific Equatorial Undercurrent: Modeled pathways and water mass  
362 evolutions. *J. Geophys. Res.*, 116, C12044, doi: 10.1029/JC007477, 2011.  
363

- 364 Griffiths, M. L., Drysdale, R. N., Gagan, M. K., Zhao, J.-X., Ayliffe, L. K.,  
365 Hellstrom, J. C., Hantoro, W. S., Frisia, S., Feng, Y.-X., Cartwright, I., St.  
366 Pierre, E., Fischer, M., J., and Suwargadi, B. W.: Increasing Australian-  
367 Indonesian monsoon rainfall linked to early Holocene sea-level rise. *Nature*  
368 *Geosci.*, 2, 636–639, 2009.
- 369  
370 Lamy, F., Kaiser, J., Ninnemann, U., Hebbeln, D., Arz, H. W., and Stoner, J.:  
371 Antarctic timing of surface water changes off Chile and Patagonian ice  
372 sheet response. *Science*, 304, 1959-1962, 2004.
- 373  
374 Lea, D. W., Pak, D. K., and Spero, H. J.: Climate impact of late Quaternary  
375 equatorial Pacific sea surface temperature variations. *Science*, 289, 1719-  
376 1724, 2000.
- 377  
378 Lea, D. W., Pak, D. K., Peterson, L. C., and Hughen, K. A.: Synchronicity of  
379 tropical high-latitude Atlantic temperatures over the last glacial termination.  
380 *Science*, 301, 1361-1364, 2003.
- 381  
382 Leduc, G., Schneider, R., Kim, J.H., and Lohmann, G.: Holocene and Eemian  
383 sea surface temperature trends as revealed by alkenone and Mg/Ca  
384 paleothermometry. *Quaternary Sci. Rev.*, 29, 989 – 1004, 2010.
- 385  
386 Levi, C., Labeyrie, L., Bassinot, F., Guichard, F., Cortijo, E., Waelbroeck, C.,  
387 Caillon, N., Duprat, J., de Garidel-Thoron, T., and Elderfield, H.: Low-  
388 latitude hydrological cycle and rapid climate changes during the last  
389 deglaciation. *Geochem., Geophys., Geosy.*, 8(5), Q05N12, doi:  
390 10.1029/2006GC001514, 2007.
- 391  
392 Linsley, B. K., Rosenthal, Y., and Oppo, D. W.: Holocene evolution of the  
393 Indonesian throughflow and the western Pacific warm Pool. *Nature Geosci.*,  
394 3, 578–583, 2010.
- 395  
396 Lo, L., Lai, Y.-H., Wei, K.-Y., Lin, Y.-S., Mii, H.-S., Shen, C.-C.: Persistent sea  
397 surface temperature and declined sea surface salinity in the northwestern  
398 tropical Pacific over the past 7500 years. *J. Asian Earth Sci.*, 66, 234-239,  
399 2013.
- 400  
401 Lo, L., Shen, C.-C., Lu, C.-J., Chen, Y.-C., Chang, C.-C., Wei, K.-Y., Qu, D.,  
402 and Gagan, M. K.: Determination of element/Ca ratios in foraminifera and  
403 corals using cold- and hot-plasma techniques in inductively coupled plasma  
404 sector field mass spectrometry. *J. Asian Earth Sci.*, 81, 115-122, 2014.
- 405  
406 McGee, D., Donohoe, A., Marshall, J., and Ferreira, D.: Changes in ITCZ  
407 location and cross-equatorial heat transport at the Last Glacial Maximum,  
408 Heinrich Stadial 1, and the mid-Holocene. *Earth Planet. Sci. Lett.*, 390, 69-  
409 79, 2014.
- 410  
411 Meckler, A. N., Clarkson, M. O., Cobb, K. M., Sodemann, H., and Adkins, J. F.:  
412 Interglacial hydroclimate in the tropical West Pacific through the late  
413 Pleistocene. *Science*, 336, 1301-1304, 2012.



- 414  
415 Melet, A., Verron, J., Gourdeau, L., and Koch-Larrouy, A.: Equatorial  
416 pathways of Solomon Sea water masses and their modification. *J. Phys.*  
417 *Oceano.*, 40, 810–826, 2011.
- 418  
419 Mohtadi, M., Oppo, D. W., Steinke, S., Stuut, J.-B. W., De Pol-Holz, R.,  
420 Hebbeln, D., and Lückge, A.: Glacial to Holocene swings of the Australian-  
421 Indonesian monsoon. *Nature Geosci.*, 4, 540–544, 2011.
- 422  
423 Mohtadi, M., Prange, M., Oppo, D. W., De Pol-Holz, R., Merkel, U., Zhang, X.,  
424 Steinke, S., and Lückge, A.: North Atlantic forcing of tropical Indian Ocean  
425 climate. *Nature* 509, 76-80, 2014.
- 426  
427 Muller, J., Kylander, M., Wüst, R. A. J., Weiss, D., Martinez-Cortizas, A.,  
428 LeGrande, A. N., Jennerjahn, T., Behling, H., Andreson, W. T., and  
429 Jacobson, G.: Possible evidence for wet Heinrich phases in tropical  
430 Australia: the Lynch's Crater deposit. *Quaternary Sci. Rev.*, 27, 468–475,  
431 2008.
- 432  
433 Northern Greenland Ice Core Project Members: High-resolution record of  
434 Northern Hemisphere climate extending into the last interglacial period.  
435 *Nature*, 431, 147–151, 2004.
- 436  
437 Oppo, D. W., Rosenthal, Y., and Linsley, B. K.: 2,000-year-long temperature  
438 and hydrology reconstructions from the Indo-Pacific warm pool. *Nature*,  
439 460, 1113–1116, 2009.
- 440  
441 Pahnke, K., Zahn, R., Elderfield, H., and Schulz, M.: 340,000-year centennial-  
442 scale marine record of Southern Hemisphere climatic oscillation. *Science*,  
443 301, 948-952, 2003.
- 444  
445 Pena, L. D., Cacho, I., Ferretti, P., and Hall, M. A.: El Niño-Southern  
446 Oscillation-like variability during glacial terminations and interlatitudinal  
447 teleconnections. *Paleoceanography*, 23, PA3101, doi:  
448 10.1029/2008PA001620, 2008.
- 449  
450 Qu, T., Gao, S., and Fine, R. A.: Subduction of South Pacific tropical water  
451 and its equatorward pathways as shown by a simulated passive tracer. *J.*  
452 *Phys. Oceanogr.*, 43, 1551-1565, 2013.
- 453  
454 Reimer, P. J., Baillie, M. G. L., Bard, E., Bayliss, A., Beck, J. W., Blackwell, P.  
455 G., Bronk Ramsey, C., Buck, C. E., Burr, G. S., Edwards, R. L., Friedrich,  
456 M., Grootes, P. M., Guilderson, T. P., Hajdas, I., Heaton, T. J., Hogg, A. G.,  
457 Hughen, K. A., Kaiser, K. F., Kromer, B., McCormac, F. G., Manning, S. W.,  
458 Reimer, R. W., Richards, D. A., Southon, J. R., Talamo, S., Turney, C. S.  
459 M., van der Plicht, J., and Weyhenmeyer, C. E.: INTCAL09 and MARINE09  
460 radiocarbon age calibration curves, 0-50,000 cal BP. *Radiocarbon* 51(4):  
461 1111-1150, 2009.
- 462

- 463 Reynolds, R. W., Rayner, N. A., Smith, T. M., and Stokes, D. C.: An improved  
464 in situ and satellite SST analysis for climate. *J.Clim.*, 15, 1609–1625, 2002.  
465
- 466 Rosenthal, Y., Oppo, D. W., and Linsley, B. K.: The amplitude and phasing of  
467 climate change during the last deglaciation in the Sulu Sea, western  
468 equatorial Pacific. *Geophys. Res. Lett.*, 30(8), 1428, doi:  
469 10.1029/2002GL016612, 2003.  
470
- 471 Shakun, J. D., and Carlson, A. E.: A global perspective on Last Glacial  
472 maximum to Holocene climate change. *Quaternary Sci. Rev.*, 29, 1801-  
473 1816, 2010.  
474
- 475 Shakun, J. D., Clark, P. U., He, F., Marcott, S. A., Mix, A. C., Liu, Z., Otto-  
476 Bliesner, B., Schmittner, A., and Bard, E.: Global warming preceded by  
477 increasing carbon dioxide concentrations during the last deglaciation.  
478 *Nature*, 484, 49-55, 2012  
479
- 480 Shen, C.-C., Hasting, D. W., Lee, T., Chiu, C.-H., Lee, M.-Y., Wei, K.-Y.,  
481 Edwards, R. L.: High precision glacial-interglacial benthic foraminiferal  
482 Sr/Ca records from the eastern equatorial Atlantic Ocean and Caribbean  
483 Sea. *Earth Planet. Sci. Lett.*, 190, 197-209, 2001.  
484
- 485 Shen, C.-C., Chiu, H.-Y., Chiang, H.-W., Chu, M.-F., Wei, K.-Y., Steinke, S.,  
486 Chen, M.-T., Lin, Y.-S., and Lo, L.: High precision measurements of Mg/Ca  
487 and Sr/Ca ratios in carbonates by cold plasma inductively coupled plasma  
488 quadrupole mass spectrometry. *Chem. Geol.*, 236, 339-249, 2007.  
489
- 490 Shiau, L.-J., Chen, M.-T., Clemens, S. C., Huh, C.-A., Yamamoto, M., and  
491 Yokoyama, Y.: Warm pool hydrological and terrestrial variability near  
492 southern Papua New Guinea over the past 50k. *Geophys. Res. Lett.*, 38,  
493 L00F01, doi: 10.1029/2010GL045309, 2011.  
494
- 495 Shiau, L.-J., Chen, M.-T., Huh, C.-A., Yamamoto, M., and Yokoyama, Y.:  
496 Insolation and cross-hemispheric controls on Australian monsoon variability  
497 over the past 180 ka: new evidence from off shore southeastern Papua  
498 New Guinea. *J. Quaternary Sci.*, 27, 911-920, 2012.  
499
- 500 Steinke, S., Chiu, H.-I., Yu, P.-S., Shen, C.-C., Erlenkeuser, H., Löwemark, L.,  
501 and Chen, M.-T.: On the influence of sea level and monsoon climate on the  
502 southern South China Sea freshwater budget over the past 22,000 years.  
503 *Quaternary Sci. Rev.*, 25, 1475–1488, 2006.  
504
- 505 Stenni, B., Jouzel, J., Masson-Delmotte, V., Röthlisberger, R., Castellano, E.,  
506 Cattani, O., Falourd, S., Johnsen, S. J., Longinelli, A., Sachs, J. P., Selmo,  
507 E., Souchez, R., Steffensen, J. P., Udisti, R.: A late-glacial high-resolution  
508 site and source temperature record derived from EPICA Dome C isotope  
509 records (East Antarctica). *Earth Planet. Sci. Lett.*, 217, 183–195, 2003.  
510

- 511 Stott, L., Cannariato, K., Thunell, R., Haug, G. H., Koutavas, A., and Lund, S.:  
512 Decline of surface temperature and salinity in the western tropical Pacific  
513 Ocean in the Holocene epoch. *Nature*, 431, 56–59, 2004.  
514
- 515 Stott, L., Poulsen, C., Lund, S., and Thunell, R.: Super ENSO and global  
516 climate oscillations at millennial time scales. *Science*, 297, 222-226, 2002.  
517
- 518 Stuiver, M., Reimer, P. J., and Reimer, R. W.: CALIB 6.0. (WWW program  
519 and documentation), 2010.  
520
- 521 Visser, K., Thunell, R., and Stott, L.: Magnitude and timing of temperature  
522 change in the Indo-Pacific warm pool during deglaciation. *Nature*, 421,  
523 152–155, 2003.  
524
- 525 Wang, Y. J., Cheng, H., Edwards, R. L., An, Z. S., Wu, J. Y., Shen, C.-C., and  
526 Dorale, J. A.: A high-resolution absolute-dated late Pleistocene monsoon  
527 record from Hulu Cave, China. *Science*, 294, 2345-2348, 2001.  
528
- 529 Wang, X., Auler, A. S., Edwards, R. L., Cheng, H., Ito, E., Wang, Y., Kong, X.,  
530 and Solheid, M.: Millennial-scale precipitation changes in southern Brazil  
531 over the past 90,000 years. *Geophys. Res. Lett.*, 34, L23701,  
532 doi:10.1029/2007GL031149, 2007.  
533
- 534 Williams, A. P, and Funk, C.: A westward extension of the warm pool leads to  
535 a westward extension of the Walker circulation, drying eastern Africa. *Clim.*  
536 *Dynam.*, 37, 2417–2435, 2011.  
537
- 538 Xu, J., Holbourn, A., Kuhnt, W., Jian, Z., and Kawamura, H.: Changes in the  
539 thermocline structure of the Indonesian outflow during Terminations I and  
540 II. *Earth Planet. Sci. Lett.*, 273, 152–162, 2008.  
541
- 542 Yan, X.-H., Ho, C.-R., Zheng, Q., and Klemas, V.: Temperature and size  
543 variabilities of the western Pacific warm pool. *Science*, 258, 1643-1645,  
544 1992.  
545

546 **Table 1** AMS <sup>14</sup>C dates of site MD05-2925.

Depth (cm)	<sup>14</sup> C ages (years)	Error (years)	Cal. ages (years)	Error (years)
117	8823	50	9414	111
127*	10306	70	11259	159
140	10441	30	11333	80
147*	11477	70	12854	110
157	12066	60	13391	84
172*	13117	70	14973	309
180	13748	35	16283	453
192*	14080	74	16746	223
207*	15616	75	18201	175
217	16470	81	19083	90
262*	18985	94	22167	181
272*	20960	150	24411	167
292*	21650	78	25304	339

547

548 \*Samples were measured in the NSF-Arizona AMS Laboratory of the  
549 University of Arizona (U. Arizona), Tucson, USA, and the others were  
550 measured in the Rafter Radiocarbon Laboratory, Institute of Geological and  
551 Nuclear Science (GNS), New Zealand.

552

553

554

555

556

557

558

559 **Table 2** Selected sites for stacked N- and S-IPWP records.

Core	Location (Latitude, and longitude)	References
North-IPWP group (orange circles in Figs 1 and 2)		
ODP 806	0.3°N, 159.4°E	Lea et al. (2000)
MD97-2140	2.0°N, 141.7°E	de Garidel-Thoron et al. (2005)
MD98-2181	6.3°N, 125.8°E	Stott et al. (2002, 2004)
MD06-3067	6.5°N, 126.5°E	Bolliet et al. (2011)
MD97-2141	8.8°N, 121.3°E	Rosenthal et al. (2003)
MD01-2390	12.1°N, 113.2°E	Stenike et al. (2006)
South-IPWP group (green circles and star in Figs 1 and 2)		
MD98-2162	4.4°S, 117.5°E	Visser et al. (2003)
MD98-2176	5.0°S, 133.4°E	Stott et al. (2004)
MD05-2925	9.3°S, 151.5°E	This Study
MD98-2165	9.7°S, 118.3°E	Levi et al. (2007)
MD98-2170	10.6°S, 125.4°E	Stott et al. (2004)
MD01-2378	13.1°S, 121.7°E	Xu et al. (2008)

560

561

562 **Figure captions**

563

564 **Fig. 1.** Climatological map of the Indo-Pacific Warm Pool (IPWP) sea surface  
 565 temperature (SST, left) and precipitation (right) during 1950-2004 AD  
 566 (Reynolds et al., 2002). Upper panels are June-July-August (JJA), and lower  
 567 panels are December-January-February (DJF) averages of **(A, C)** SSTs and  
 568 **(B, D)** precipitation distribution maps. SST and precipitation are at 0.5 °C and  
 569 2 mm/day intervals. Our study site MD05-2925 is shown as the green star.  
 570 Orange and green dots denote previous study sites in the IPWP region (Table  
 571 2) for reconstruction of meridional thermal and precipitation variations during  
 572 the glacial/interglacial change.

573

574 **Fig. 2.** EOF analysis on SST (Dataset from Reynolds et al., 2002) and  
 575 selected sites (Table 2) used for stacked N- and S-IPWP records. **(A)** EOF1  
 576 explains 83.4% of the total variance, which mainly represents intra-annual  
 577 seasonality. **(B)** EOF2 shows a clear zonal pattern. Orange circles represent  
 578 selected sites for the N-IPWP group and green ones for the S-IPWP group.  
 579 The green star denotes the MD05-2925 site used in this study.

580

581 **Fig. 3.** Planktonic foraminifera *G. ruber* geochemical proxy records of site  
 582 MD05-2925, including **(A)** oxygen isotope ( $\delta^{18}\text{O}_C$ ), **(B)** Mg/Ca ratio, and **(C)**  
 583 temperature corrected-only seawater oxygen isotope ( $\delta^{18}\text{O}_{SW}$ ). Triangle  
 584 symbols are corrected radiocarbon dates (Table 1).

585

586 **Fig. 4.** Geochemical proxy records of MD05-2925. **(A)** SST (red circles and  
 587 line) and **(B)**  $\delta^{18}\text{O}_{SW-IVC}$  (blue line) were reconstructed with *G. ruber* Mg/Ca  
 588 ratios and  $\delta^{18}\text{O}_C$ . The cyan line denotes the Antarctica EPICA deuterium  
 589 isotope record (Stenni et al., 2003), and the yellow line is the Greenland ice  
 590 core NGRIP (Northern Greenland Ice Core Project Members, 2004) oxygen  
 591 isotope record. The superimposed dark cyan and dark yellow lines are the  
 592 200-yr smoothed records, respectively. Black triangles are AMS  $^{14}\text{C}$  dates  
 593 (Table 1). Vertical bars denote the H1 and YD periods.

594

595 **Fig. 5.** Four hundred-year non-overlapping binned **(A)** SST and **(C)**  $\delta^{18}\text{O}_{SW-IVC}$   
 596 of N- (orange solid line) and S-IPWP (green solid line). Lower panel show the  
 597 differences in **(B)** SST and **(D)**  $\delta^{18}\text{O}_{SW-IVC}$  between N- and S-IPWP. The  
 598 compilations of N- and S-IPWP surface water thermal and hydrological  
 599 records (Table 2) were calculated with the non-overlapping binned methods  
 600 (Oppo et al., 2009; Linsley et al., 2010). All dashed lines represent 1-sigma  
 601 uncertainty ranges. Gray bars show the H1 and YD events.

602

603 **Fig. 6.** Hypothetical proxy-inferred precipitation boundary during the H1 and  
 604 YD events (modified from the Linsley et al., 2010). Blue dots represent  
 605 relatively increasing precipitation/ $\delta^{18}\text{O}_{SW}$  lighter condition, and brown ones a  
 606 decreasing precipitation/ $\delta^{18}\text{O}_{SW}$  heavier condition. The segment between  
 607 Java and Flores Islands of this sharp boundary (red dashed line) was  
 608 proposed by Mohtadi et al. (2011), and the one between the Solomon and  
 609 Coral Seas by this study. Black contours represent SST.

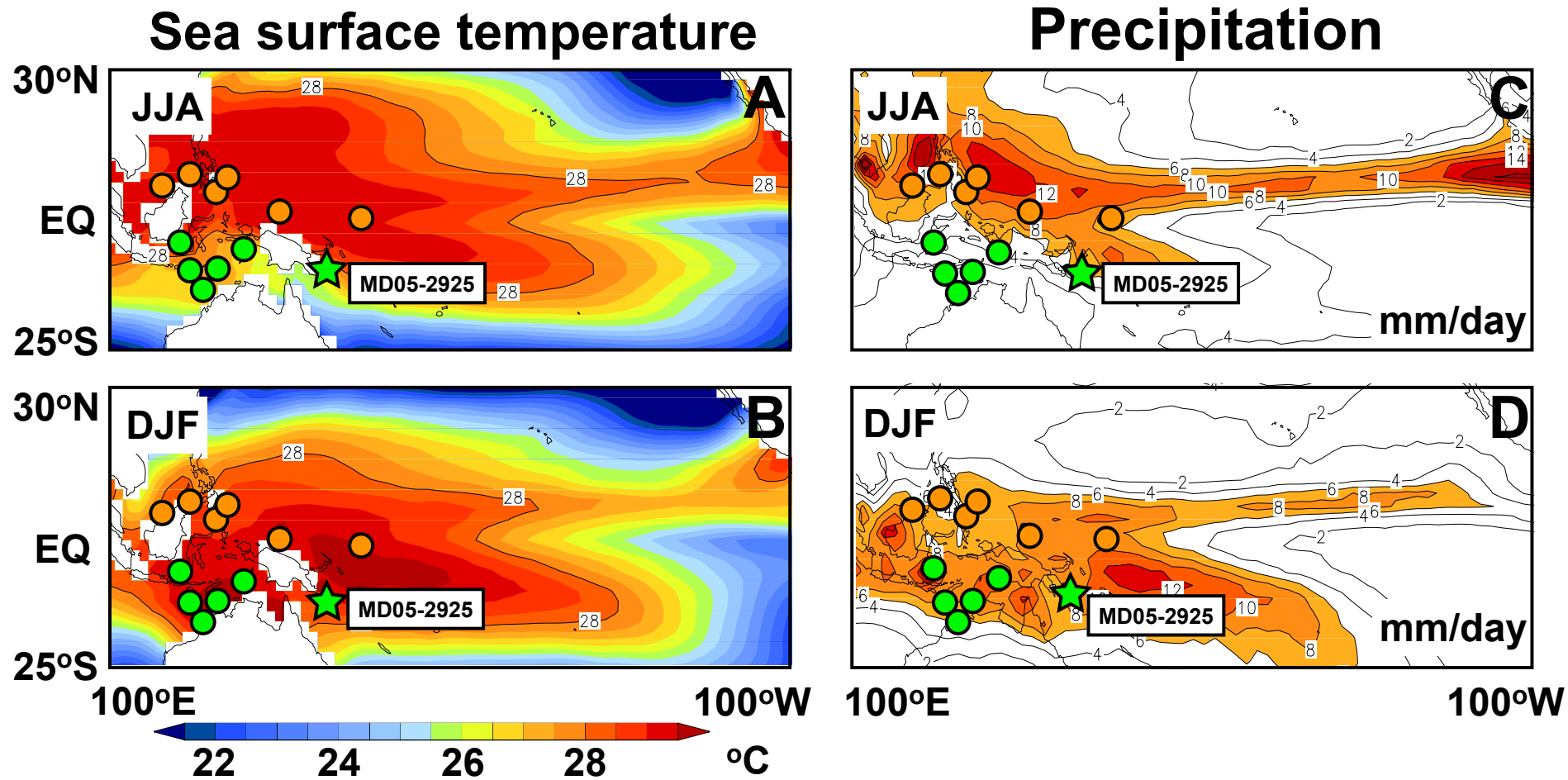


**Fig. 1**

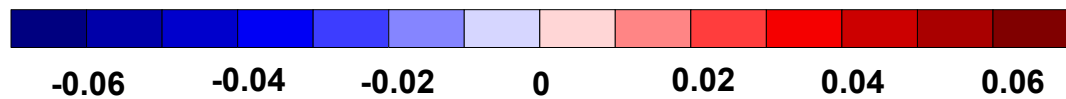
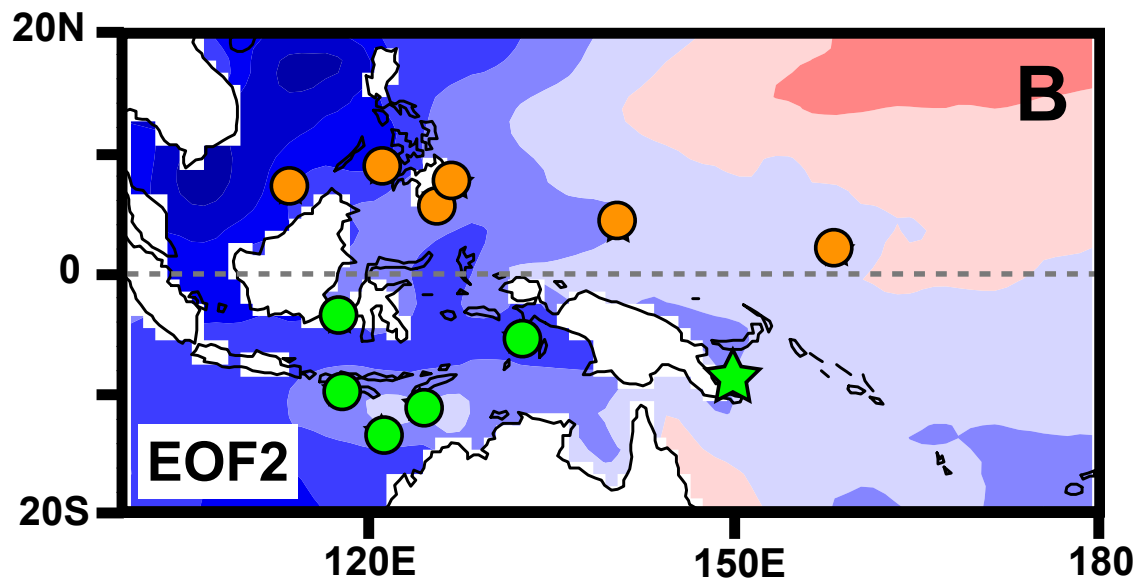
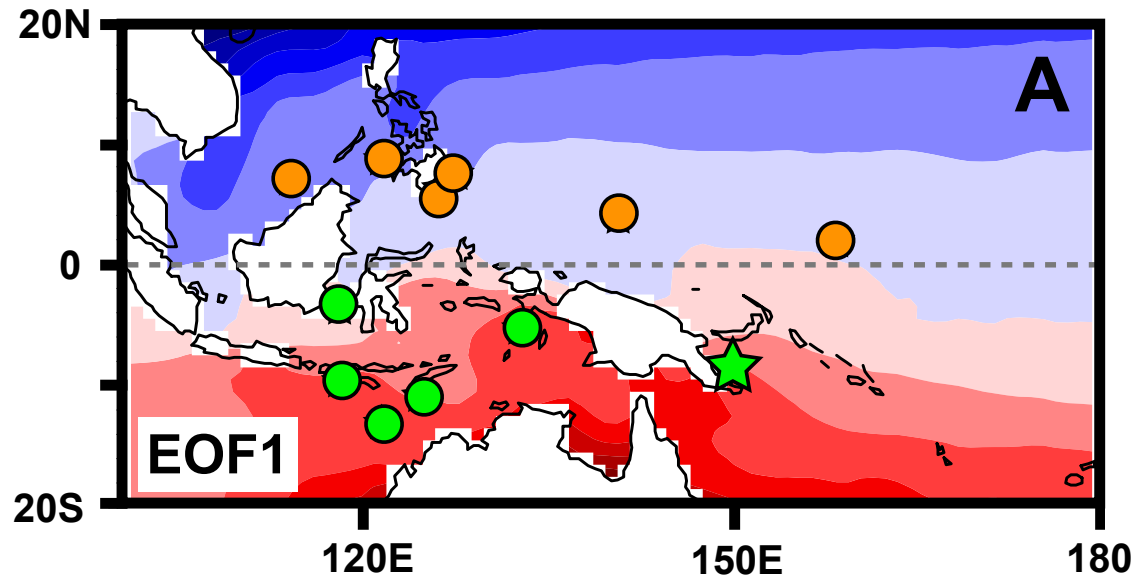


**Fig. 2**



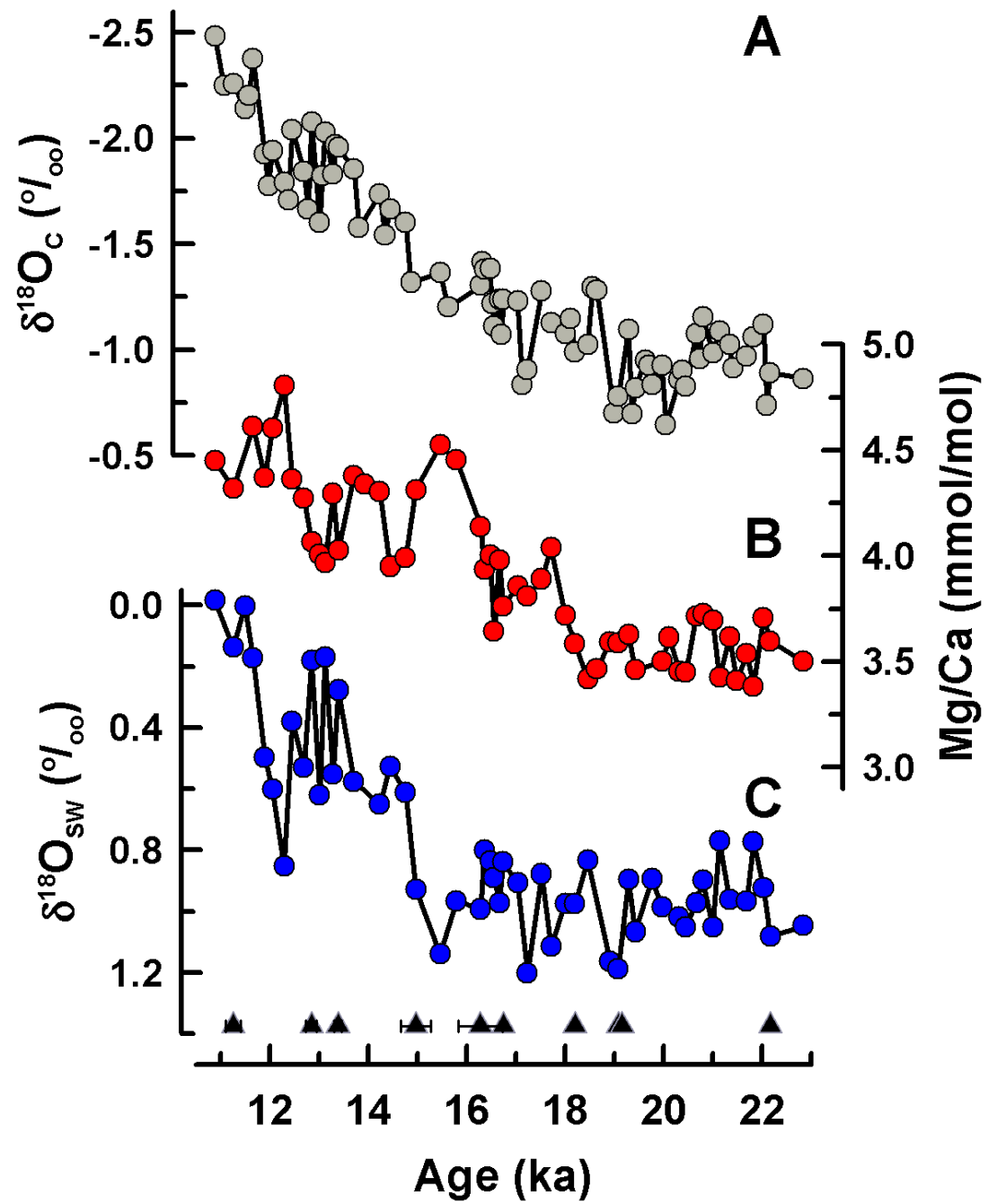


**Fig. 3**

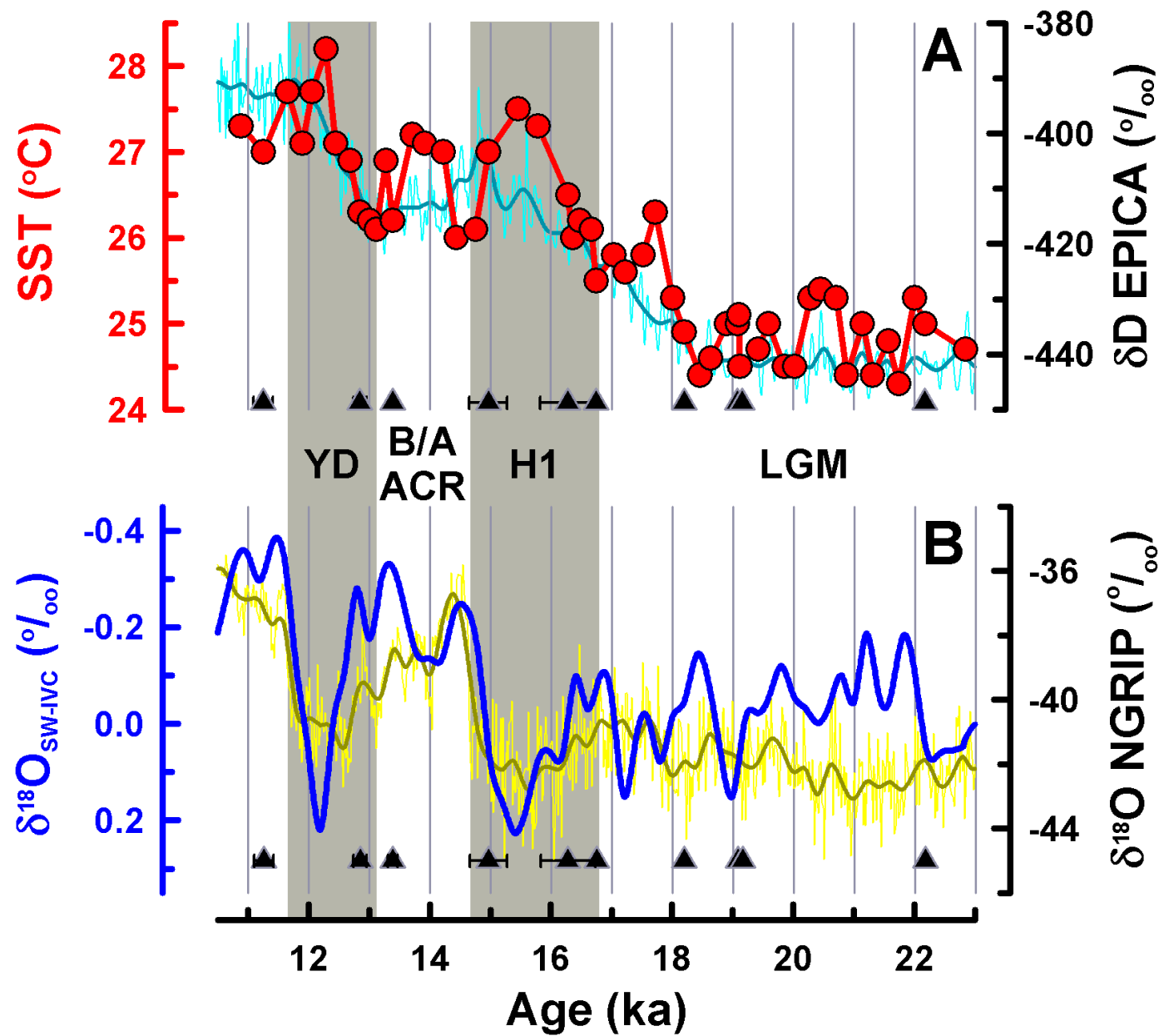


**Fig. 4**

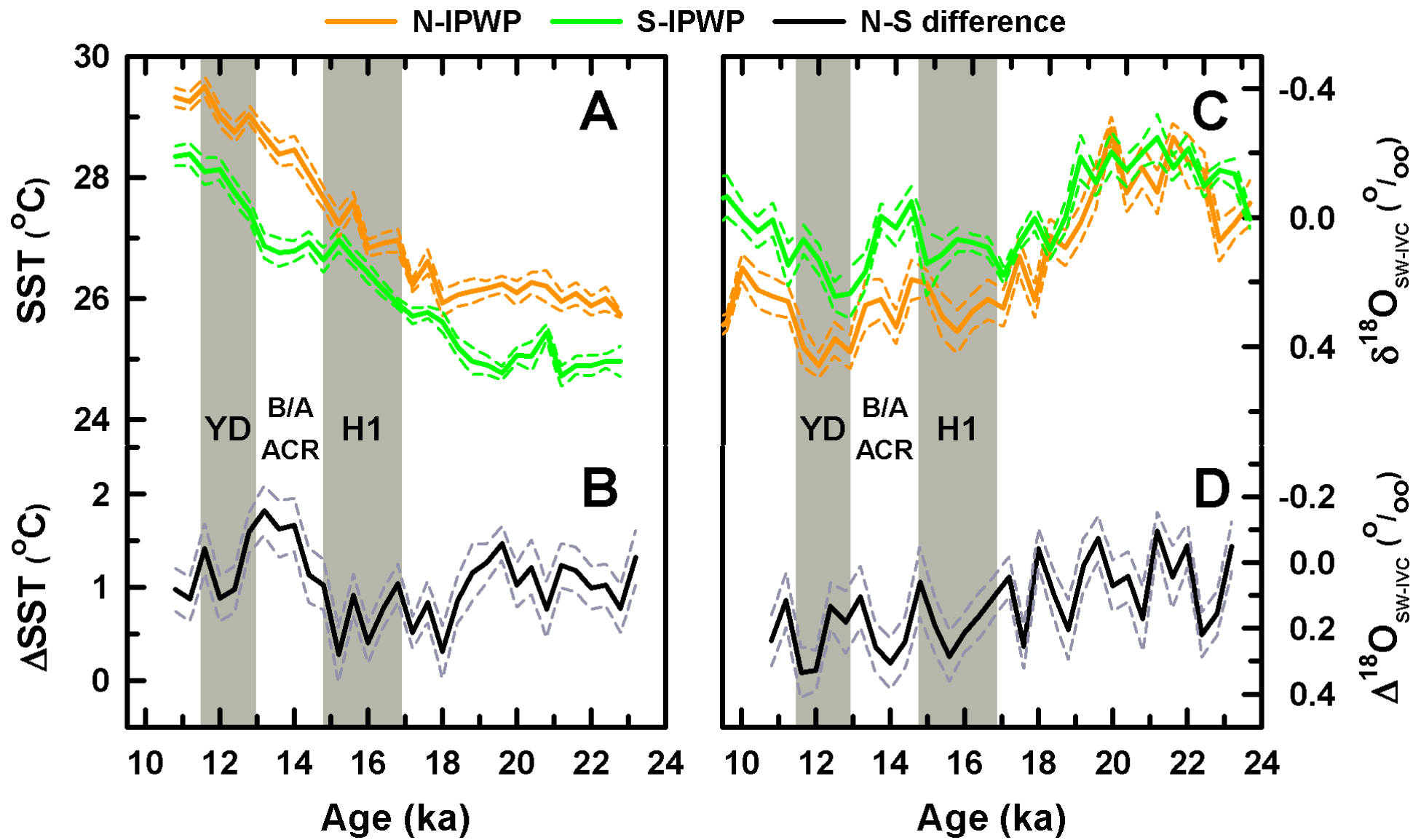


**Fig. 5**

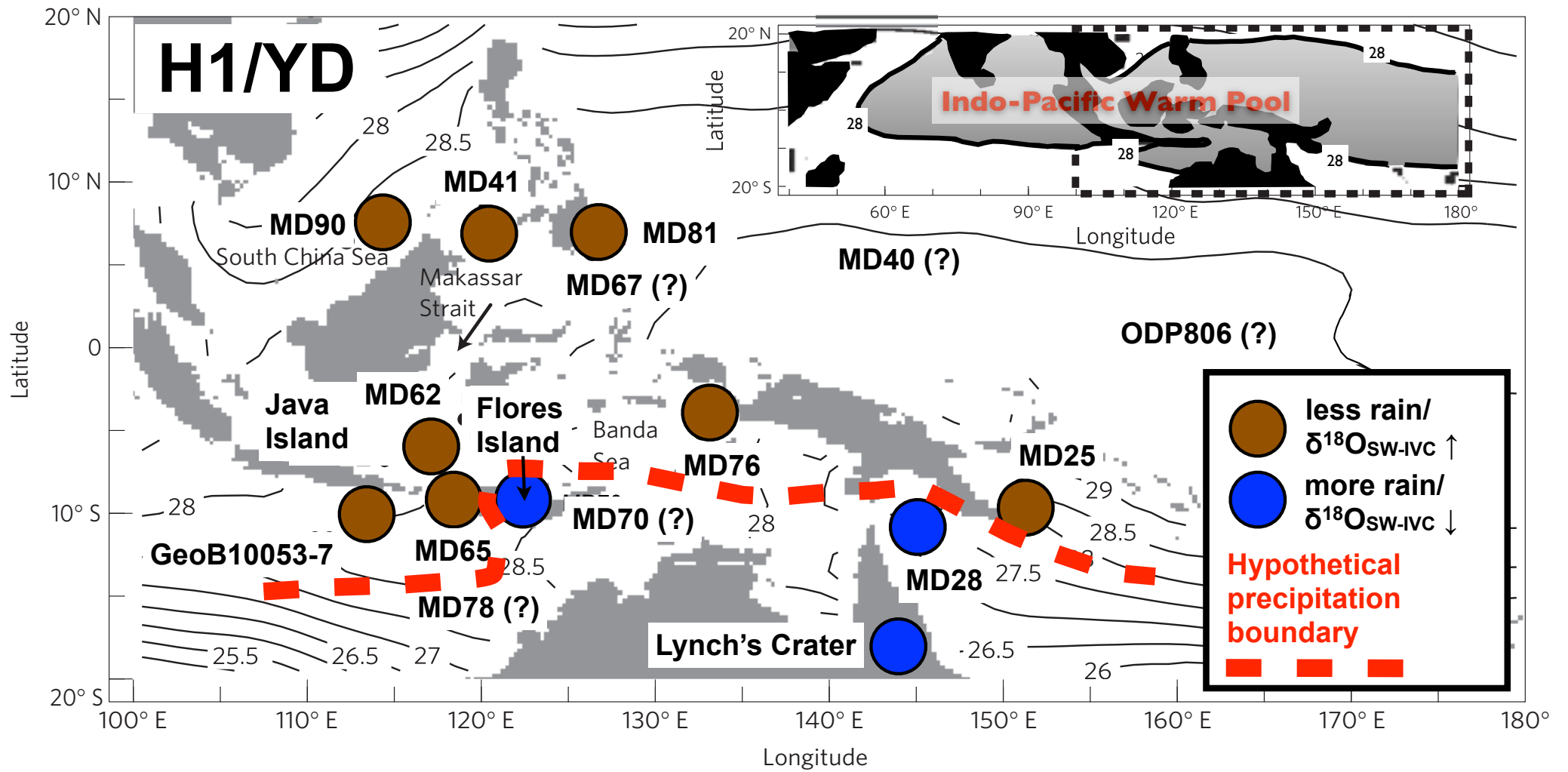


**Fig. 6**